

Some applications of TDA on financial markets

Miguel Angel Ruiz-Ortiz¹, José Carlos Gómez-Larrañaga², and
Jesús Rodríguez-Viorato³

¹Universidad de Guanajuato, Guanajuato 36240, Gto., MÉXICO;
miguel.ruiz@cimat.mx

²CIMAT, A.P. 402, Guanajuato 36000, Gto., MÉXICO; jcarlos@cimat.mx

³CIMAT, A.P. 402, Guanajuato 36000, Gto., MÉXICO; jesusr@cimat.mx

May 10, 2022

Abstract

The Topological Data Analysis (TDA) has had many applications. However, financial markets has been studied slightly through TDA. Here we present a quick review of some recent applications of TDA on financial markets and propose a new turbulence index based on persistent homology — the fundamental tool for TDA — that seems to capture critical transitions on financial data, based on our experiment with SP500 data before 2020 stock market crash in February 20, 2020, due to the COVID-19 pandemic. We review applications in the early detection of turbulence periods in financial markets and how TDA can help to get new insights while investing and obtain superior risk-adjusted returns compared with investing strategies using classical turbulence indices as VIX and the Chow’s index based on the *Mahalanobis* distance. Furthermore, we include an introduction to persistent homology so the reader could be able to understand this paper without knowing TDA.

Keywords: TDA, Financial Markets, Time Series, Persistence Homology, Persistence Diagrams, Persistence Landscapes

1 Introduction

The main objective of Topological Data Analysis (**TDA**) is to find the *shape of data*, checking if there are connected components, holes or gaps in a representation of data in \mathbb{R}^d . This has been achieved mainly through **persistent homology** ([4, 7]) and it deals with the detection of n -dimensional holes, $n = 0, 1, 2, \dots$, that are formed by connecting nearby points.

There are at least two good reasons for using persistent homology applied to financial data. First, financial data is high dimensional and persistent homology gives us insights about the shape of data even if we cannot visualize financial

data in a high dimensional space. Second, persistent homology is robust to perturbations of input data, and this robustness is ideal for reliable prediction of regime shifts in markets ([15, 1]).

In this paper we review what kind of efforts have been done to understand financial markets via TDA and how TDA could help us to control risk while investing on financial markets. Furthermore, we propose a new turbulence index based on persistent homology based on previous ideas ([10, 1]). We found that applications in financial markets are in their early stages of development at the time this research was done (see [9, 11, 10, 22, 1]). A common way of studying financial markets is through the time series given by the prices of financial assets. As can be seen in [17], the application of TDA to time series is relatively new, and deals with areas such as dynamic systems and signal processing (see [16, 2]).

In section 2, we find an introduction to persistent homology —the main tool of TDA — together with some theoretical concepts to fully understand the applications to financial markets explained here. In general, the main application of TDA in financial markets has been the study of **critical transitions**, which are the applications on which we focus the most here. By critical transition we mean an abrupt change in the behavior of a complex system. A critical transition in financial markets is known as a market **crash**.

In section 3, we detail three applications of TDA to the detection of critical transitions in financial markets ([9, 11, 10]). Getting early signs of a critical transitions in financial markets would help to gain better control of risk in portfolio construction. This, however, is a challenging task as [9] mentions.

In section 4, the development of investing strategies by [1] based on a persistent homology based turbulence index (PHTI) is examined. Finally, in section 5, we propose a modified version of the PHTI and see how this index can capture the abrupt change in S&P500 prices due to the 2020 stock market crash between February 20 and April 7 of 2020 induced by the COVID-19 pandemic.

1.1 Financial markets concepts

A **financial asset** is an investing vehicle. Some examples of financial assets are shares of stocks, bonds, foreign currencies and real state. The three main characteristics of financial assets are liquidity (capacity of converting the asset into money), a profit and risk. The price of these assets follows the laws of supply and demand, so price fluctuates over time. A **portfolio** is simply a collection of financial assets. These assets are acquired in the **financial markets** (stock market, foreign exchange market, or cryptocurrency market).

We may buy a financial asset, for example, shares of a company, with the goal in mind of obtaining a profitability. This can be achieved if the price of this financial asset increases after we have bought it and then we sell it. Transactions of financial assets have the risk of having losses instead of returns, because the price may decrease after we have bought it.

Due to the volatility and uncertainty that often exist in financial markets, it is important to have risk measures to avoid large losses caused by extreme

market movements. This topic has been widely studied with statistics and artificial intelligence tools (see [14, 21]).

2 Persistence Homology

This section introduces the TDA concepts necessary to understand this dissertation. To go deeper, see [4, 7, 8].

2.1 Simplicial Homology

Definition: A **simplicial complex** Σ is a collection of non-empty subsets of a finite set of vertices Σ_0 that satisfy

$$\alpha \in \Sigma, \beta \subset \alpha \Rightarrow \beta \in \Sigma.$$

If $\alpha \in \Sigma$ and $k = |\alpha| - 1$, α is called a k - **simplex**, and $\beta \subset \alpha$ is known as a **face** of α . We will denote the set of all k -simplices as Σ_k . The **dimension** of Σ is defined as

$$\dim(\Sigma) := \max_{\alpha \in \Sigma} \{|\alpha| - 1\}.$$

These concepts can be visualized in figure 1. In TDA, simplices are used to study data.

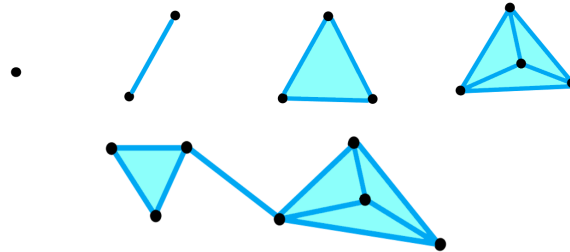


Figure 1: k -simplices for $k = 0, 1, 2, 3$ (top) and a simplicial complex (bottom).

Let us consider C_k the free abelian group with coefficients in \mathbb{Z} generated by the k -simplices, so each element $c \in C_k$ can be expressed as

$$c = \sum_{i=1}^n c_i \alpha_i,$$

where the α_i are k -simplices and $c_i \in \mathbb{Z}$, for some $n \in \mathbb{N}$.

Suppose that a total order is imposed on the set of vertices Σ_0 . This allows defining a set of homomorphisms $d_i : \Sigma_k \rightarrow \Sigma_{k-1}$, $0 \leq i \leq k$, given by

$d_i(\sigma) = \sigma \setminus \{s_i\}$, where s_i is the i -th element of σ . Let us define the *boundary homomorphism* $\delta_k : C_k \rightarrow C_{k-1}$ given by

$$\delta_k = \sum_{i=0}^k (-1)^i d_i.$$

Notice that $\delta_k \circ \delta_{k+1} = 0$, so $Im(\delta_{k+1}) \subseteq Ker(\delta_k)$. This leads to the following definition.

Definition: The k -th homology group of Σ is defined as

$$H_k(\Sigma) = Ker(\delta_k) / Im(\delta_{k+1}).$$

The k -th Betti number of Σ is defined as

$$\beta_k = rank(H_k(\Sigma)),$$

and it is the number of k -dimensional holes on Σ , e.g., β_0 is the number of independent connected components, β_1 is the number of loops, β_2 is the number of cavities, and so on.

2.2 Construction of simplicial complexes

Suppose we have a point cloud $X = \{x_1, x_2, \dots, x_N\} \subset \mathbb{R}^d$. We would like to associate X with a simplicial complex to study its shape. The following are some different ways to do it.

2.2.1 Čech simplicial complex

Definition: The *Čech complex* $C(X, \epsilon)$ with parameter $\epsilon > 0$ and with vertices in X is

$$C(X, \epsilon) = \left\{ \alpha \subset X : \bigcap_{v \in \alpha} B_\epsilon(v) \neq \emptyset \right\}$$

where $B_\epsilon(v)$ is the ball of radius ϵ centered at v . This simplicial complex is called the *nerve* of $\{B_\epsilon(x)\}_{x \in X}$.

2.2.2 Vietoris-Rips simplicial complex

Definition: The *Vietoris-Rips complex* $VR(X, \epsilon)$ with parameter $\epsilon > 0$ and with vertices in X is

$$VR(X, \epsilon) = \{ \alpha \subset X : \|v_i - v_j\| \leq \epsilon, \forall v_i, v_j \in \alpha \}.$$

Notice that if $\Sigma(\epsilon)$ is the Čech complex or the Vietoris-Rips complex associated with $\epsilon > 0$ with vertices at X , we get

$$\Sigma(\epsilon') \subseteq \Sigma(\epsilon), \quad \forall \epsilon' \leq \epsilon.$$

We call this the **filtering property**. For this property it follows that:

$$H_k(\Sigma(\epsilon')) \hookrightarrow H_k(\Sigma(\epsilon)), \quad \forall \epsilon' \leq \epsilon.$$

These last two results are helpful for the definition of persistent homology, as we will see later.

2.2.3 Clique simplicial complex

Sometimes the data is presented through a graph $G = (V, E)$, where V is the set of vertices and E is the set of edges. An example of this is the correlation networks used in [9] (see section 3.1).

Definition: Given a graph $G = (V, E)$, a *clique* C is a set of vertices of V such that every pair of different vertices in C are connected by an edge at E .

With the previous definition, it is now possible to define the clique complex (see [12]).

Definition: Let $G = (V, E)$ be a graph. The *clique complex* $X(G)$ of G is the simplicial complex resulting from considering each clique with k vertices as a $(k - 1)$ -simplex.

Suppose there is a function $w : E \rightarrow [0, \infty)$ that assigns a weight to each edge of G —i.e., G is a *weighted graph*. Let us consider $\theta_{max} = \max(w)$ and $\theta \in [0, \theta_{max}]$. Let $G(\theta)$ be the subgraph of G that keeps all edges with weights less than or equal to θ . Note that if $0 \leq \theta' \leq \theta$, then $G(\theta') \subset G(\theta)$ (the former is subgraph of the latter). Even more,

$$X(G(\theta')) \subseteq X(G(\theta)),$$

that is, the filtering property is obtained.

2.3 Persistent homology

2.3.1 Filtration

Definition: Let Σ be a simplicial complex. A *filtration* of Σ is a mapping $\epsilon \in (0, \infty) \mapsto \Sigma(\epsilon)$, where $\Sigma(\epsilon) \subseteq \Sigma$ is also a sub-simplicial complex and fulfills the *filtering property*:

$$\Sigma(\epsilon') \subseteq \Sigma(\epsilon), \quad \forall \epsilon' \leq \epsilon.$$

We have already commented that a filtration $\epsilon \mapsto \Sigma(\epsilon)$ induces the following property in the homology groups:

$$H_k(\Sigma(\epsilon')) \hookrightarrow H_k(\Sigma(\epsilon)), \quad \forall \epsilon' \leq \epsilon.$$

This induces a canonical homomorphisms $h_k^{\epsilon', \epsilon} : H_k(\Sigma(\epsilon')) \rightarrow H_k(\Sigma(\epsilon))$, for all k and $\epsilon' \leq \epsilon$ induced by the inclusion. For the following definitions, let us consider a filtration $\epsilon \mapsto \Sigma(\epsilon)$.

Definition: The *k-th persistent homology groups* are given by $H_k^{\epsilon', \epsilon} = \text{Im}(h_k^{\epsilon', \epsilon})$, $\forall \epsilon' \leq \epsilon$.

Definition: We say that the homology class $\alpha \in H_k(\Sigma(b))$, $b > 0$, is *born* in b if $\alpha \notin H_k^{b-\delta, b}$ for all $\delta > 0$. If α is born in b , we say that *dies* in $d \geq b$ if $h_k^{b, \epsilon}(\alpha) \neq 0$ for $b < \epsilon < d$, and $h_k^{b, d}(\alpha) = 0$. If α is born and never dies in the above sense, we say that *dies in* $d = \infty$.

We then have a birth value $b(\alpha) = b$ and a death value $d(\alpha) = d$ for each α in the homology groups.

Definition: The *persistence*, or *lifetime*, of the homology class α is the difference

$$\text{pers}(\alpha) = d(\alpha) - b(\alpha).$$

The intuition behind these concepts is that through a “discrete” filtration of simplicial complexes associated with a finite number of parameters $0 < \epsilon_1 < \epsilon_2 < \dots < \epsilon_n$ we can track the topological characteristics (connected components, holes, etc.) that appear throughout the filtration (see figure 2). Those generators that have more persistence are the most significant.

2.4 Persistence Diagrams

Definition: Let us fix a basis for each homology group. The k -th *persistence diagram* (or k -dimensional persistence diagram) of the filtration $\epsilon \mapsto \Sigma(\epsilon)$ is defined as the multiset P_k in \mathbb{R}^2 obtained as follows:

- Each generator class α_k in a k -th homology group is assigned a point $(b_k, d_k) \in \mathbb{R}^2$ with multiplicity $\mu_k(b_k, d_k)$, where $b_k = b(\alpha_k)$ and $d_k = d(\alpha_k)$ (the birth and death parameters), and the multiplicity is the number of generators α_k that were born in b_k and died in d_k .
- P_k contains all points $(x, x) \in \mathbb{R}^2$ with $x \geq 0$.

Notice the dependence between the persistent diagrams and the basis chosen for each homology group.

2.4.1 Distance between persistence diagrams

The persistence diagram space \mathcal{P} can be given a metric space structure. A standard metric is the following.

Definition: The *Wasserstein distance* of degree p , $p > 0$, is defined as

$$W_p(P_k^1, P_k^2) = \inf_{\phi} \left[\sum_{q \in P_k^1} \|q - \phi(q)\|_{\infty}^p \right]^{1/p},$$

where the infimum is taken over all bijections $\phi : P_k^1 \rightarrow P_k^2$, and $\|\cdot\|_{\infty}$ denotes the supremum norm at \mathbb{R}^2 . When $p = \infty$, the Wasserstein distance W_{∞} is known as the *bottleneck distance*.

An important property that makes persistent homology suitable for analyzing data with noise is its robustness under small disturbances in the data. That is, if our point cloud we are studying changes ‘a little’, then the Wasserstein distance between the respective persistence diagrams is small (see [6]).

2.5 Persistence landscapes

The metric space (\mathcal{P}, W_p) that we already defined is not complete, so it is not suitable for statistical purposes. This is why *persistence landscapes* are defined, which are elements in the Banach space $L^p(\mathbb{N} \times \mathbb{R})$, in which statistical methods can be used (see [3]).

Let us consider P a persistence diagram. For each point $(b_\alpha, d_\alpha) \in P$ associated to the birth and death of some homological class α , define

$$f_{(b_\alpha, d_\alpha)}(x) = \begin{cases} x - b_\alpha, & x \in (b_\alpha, \frac{b_\alpha + d_\alpha}{2}] ; \\ -x + d_\alpha, & x \in (\frac{b_\alpha + d_\alpha}{2}, d_\alpha) ; \\ 0, & x \notin (b_\alpha, d_\alpha). \end{cases}$$

Let us $\lambda = (\lambda_k)_{k \in \mathbb{N}}$ be a sequence of functions $\lambda_k : \mathbb{R} \rightarrow [0, \infty)$ given by

$$\lambda_k(x) = k\text{-max}\{f_{(b_\alpha, d_\alpha)}(x) : (b_\alpha, d_\alpha) \in P\},$$

where $k\text{-max}$ denotes the k -th largest value of a function. When the k -th largest value does not exist, we set $\lambda_k(x) = 0$.

Definition: The *persistence landscape* associated with the persistence diagram P is the sequence of functions $\lambda = (\lambda_k)_k \in L^p(\mathbb{N} \times \mathbb{R})$ defined above. λ_k is known as the k -th layer of the persistence landscape.

The norm that we consider in the Banach space $L^p(\mathbb{N} \times \mathbb{R})$ is given by

$$\|\eta\|_p = \left(\sum_{k=1}^{\infty} \|\eta_k\|_p^p \right)^{1/p},$$

where $\eta = (\eta_k)_k$ and $\|\cdot\|_p$ denotes the norm L^p , i.e.,

$$\|f\|_p = \left(\int_{\mathbb{R}} |f|^p \right)^{1/p}.$$

For an example of how persistence landscapes look like, see figure 2.

3 Detecting critical transitions

3.1 Correlation graphs of Dow-Jones index

[9] studied the daily returns of company stocks in the Dow Jones Industrial Average (DJIA) during the period January 2004 to September 2008 and tracks the change in the topology of the **correlation graphs**, defined below, as prices approached the 2007-2008 financial crisis using persistent homology and persistence diagrams. Their objective was to find early signs of such a critical transition—a crash—in financial markets.

Let us consider $x_i(t)$ the daily return t of the i -th share. The graph $G = (V, E)$ of correlation at time t of the returns $\{x_i(t)\}_{t,i}$ is a weighted graph where

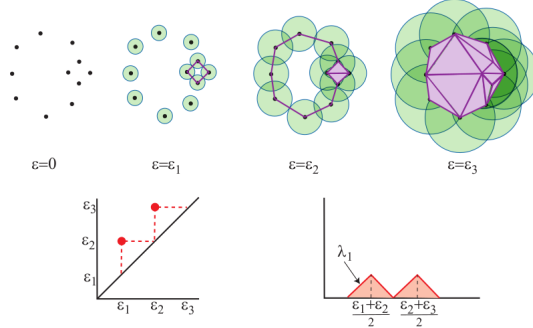


Figure 2: Filtration of Vietoris-Rips simplicial complexes (above) together with the 1-dimensional persistence diagram and the corresponding 1-st layer of its persistence landscape. Image taken from [11]

the actions of the DJIA are the vertices V , and each pair of distinct vertices $i, j \in V$ are connected by an edge $e \in E$, which is assigned the weight

$$d_{i,j}(t) := \sqrt{2(1 - c_{i,j}(t))},$$

where

$$c_{i,j}(t) = \frac{\sum_{\tau=t-T}^t (x_i(\tau) - \bar{x}_i)(x_j(\tau) - \bar{x}_j)}{\sqrt{\sum_{\tau=t-T}^t (x_i(\tau) - \bar{x}_i)^2} \sqrt{\sum_{\tau=t-T}^t (x_j(\tau) - \bar{x}_j)^2}},$$

is the Pearson correlation coefficient between nodes i and j at time t with a time window T , and \bar{x}_i, \bar{x}_j are the average of the returns of the action i and j in that time window. The author used $T = 15$.

According to the section 2.2.3, for each t we can compute the persistent homology of the correlation graph at time t and obtain information about its topology. The author computed the persistent homology in dimensions 0 and 1. His results showed how there is less correlation between stocks before the 2008 financial crash and the correlation between stocks was increasing days before the crisis. This was quantified with the Wasserstein distances between the 0-dimensional persistence diagrams at time t and at an initial time t_0 . In this time series of distances the author found greater oscillations days before the crash, thus having signs of the critical transition.

3.2 Persistence landscapes of financial crashes

[11] studied the daily returns of the S&P500, the DJIA, NASDAQ and the Russel 2000 —the 4 major financial indices in the United States— during the technology crash of 2000 and the financial crisis of 2008. Each 1-dimensional time series together form a 4-dimensional time series. The authors used persistent homology to detect topological patterns in this multidimensional time

series. Persistence landscapes and their norms L^p , $p = 1, 2$, were used to measure changes in 1-dimensional persistence diagrams. In their results, they found that the L^p norms have considerable growth days before the two crashes to be considered, while the norms behave calmly when the market is stable. The methodology they used is described below.

Let $\{x_n^k\}_n$, $k = 1, \dots, d$, be d time series and let us fix a window size w . For each time t_n , we have a point $x(t_n) = (x_n^1, \dots, x_n^d) \in \mathbb{R}^d$. Let us consider the matrix

$$X_n := [x(t_n)^T, x(t_{n+1})^T, \dots, x(t_{n+w-1})^T]$$

of size $d \times w$, which represents a cloud of w points in \mathbb{R}^d . Then, we obtain a filtering of Rips simplicial complexes to obtain the persistence diagram of dimension 1 and then its associated persistence landscape together with its norm L^1 and L^2 . This is done for each time t_n , obtaining a time series of the norms of persistence landscapes that tracks changes in the topological properties of each point cloud X_n over time.

The authors found that these norms grow when periods of high volatility in the markets approach such as the crash of 2000 and 2008. They applied the methodology described before to the daily log-returns of the S&P500, the DJIA, NASDAQ and the Russel 2000 from December 23, 1987 to December 8, 2016 (7301 daily data).

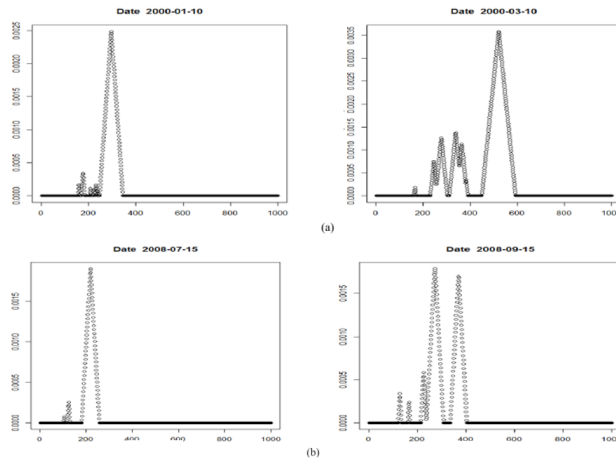


Figure 3: 1-dimensional persistence landscapes. In a) and b) we find their behavior a few days before and at the beginning of the 2000 technology crash on March 20, 2000 and the 2008 crash on September 15, 2008, respectively. Image taken from [11].

The figure 3 shows some persistence landscapes associated with the 1-dimensional persistence diagrams with information about the 1-cycles in the point clouds. In 3.a), we find the landscapes of two point clouds near the technology crash of

2000, which is considered to be on March 10, 2000. One point cloud was taken on this date and the other two months before. The same was done in 3.b) for the crash of 2008, when the bankruptcy of the Lehman Brothers company on September 15, 2008.

We can see more persistent 1-cycles emerging in the point clouds when there is more volatility in the market. To quantify this behavior, the L_1 and L_2 norms of the persistence diagrams λ were computed for each point cloud. The set of values obtained induces a daily time series with these quantities. From what we can see in figure 3, we expect that there will be an increase in the L_1 and L_2 rules as a crash approaches (see figure 4).

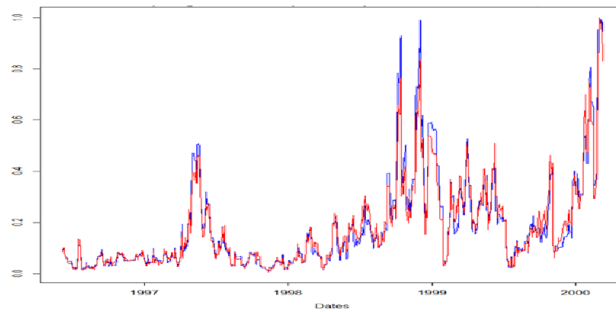


Figure 4: Normalized time series of the L_1 norms in blue and the L_2 norms in red before the crash of 2000. Image taken from [11].

To see the variability of both time series, the author proceeds to calculate the 500-day moving variance (see image 5). As expected, the time series of the moving variance also grows closer to both financial crashes.

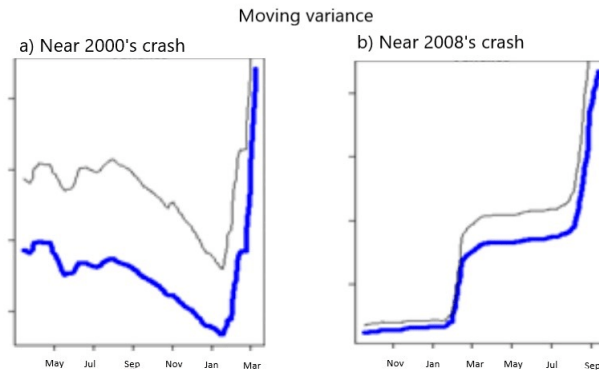


Figure 5: Moving variance of the series with the norms L_1 (in gray) and L_2 (in blue) near 2000's and 2008's crashes. Image taken from [11].

3.3 Crashes in cryptocurrency market

[10] analyzed the time series of four of the most important cryptocurrencies: Bitcoin, Ethereum, Litecoin and Ripple —which made up 66 % of the total cryptocurrency market capitalization— using a similar approach to [11]. The difference between both approaches is that the methodology of [10] was applied to a specific time series, while in [11] the methodology was applied to d time series. Furthermore, [10] took into account what they define as the C^1 norm of persistence landscapes and use the k -means algorithm of machine learning, which is a clustering algorithm, to identify patterns in prices and the C^1 norms indicating critical transitions before the *cryptocurrency crash* in January 2008, which started with a Bitcoin price drop of 65%.

The methodology of [10] was the following. Let us consider a time series $X = \{x_0, \dots, x_{N-1}\}$ and set $d \in \mathbb{N}$. Let

$$z_t := (x_t, x_{t+1}, \dots, x_{t+d-1}) \in \mathbb{R}^d,$$

for $t \in \{0, \dots, N-d\}$. We now have a sequence of point clouds in \mathbb{R}^d

$$Z^t := \{z_t, z_{t+1}, \dots, z_{t+(w-1)}\}, \quad t \in \{0, \dots, N-d-w+1\},$$

where w is the size of a sliding window (the number of points in each cloud). This association between the time series and the sequence of point clouds is known as the **time-delay coordinate embedding** or **Takens' embedding**, which is inspired by Takens' theorem (see [19]).

Let us fix $t \in \{0, \dots, N-d-w+1\}$ and consider the point cloud Z_t . We obtain a filtration of Vietoris-Rips simplicial complexes to obtain the 1-dimensional persistence diagram, its persistence landscape λ^t , and the norm L^1 of this latter. In this way, we obtain a time series $\{\|\lambda^t\|_1\}_t$.

To detect the cases when $\|\lambda^t\|_1$ is large or when there are large jumps between $\|\lambda^t\|_1$ and $\|\lambda^{t-1}\|_1$, the authors define the *norm* C^1 of the persistence landscape λ^t as

$$\|\lambda^t\|_{C^1} = \|\lambda^t\|_1 + \left| \|\lambda^t\|_1 - \|\lambda^{t-1}\|_1 \right|,$$

which is a definition motivated by the C^1 norm of differentiable functions. Notice that $\|\cdot\|_{C^1}$ is not a norm but just a quantity to identify the patterns of $\|\lambda^t\|_1$ of interest.

This series of steps were applied to the daily log-returns of Bitcoin, Ethereum, Litecoin and Ripple from September 14th, 2017, until the most significant previous peak to the critical transition in each cryptocurrency. They took $d = 4$ and $w = 50$ in their experiments.

The k -means algorithm was applied to the points $\{(x_t, y_t)\}_t$, where x_t is the logarithm of the price at time t of a cryptocurrency and $y_t = \|\lambda^t\|_{C^1}$ is the norm C^1 of the persistence landscape λ^t . Both time series $\{x_t\}_t$ and $\{y_t\}_t$ were scaled to the interval $[0, 1]$ prior to this algorithm. k was chosen using the *elbow method* ([13]).

A cluster given by the k -means algorithm was defined as a **early warning signal** if the cluster contained points (x_t, y_t) with $y_t > 0.5$ and the times t

formed an almost contiguous time interval. If most of the points has $y_t > 0.5$, it was a **strong early warning signal**; and if only a few points had $y_t > 0.5$, it was a **weak early warning signal**.

For the cryptocurrencies Bitcoin, Ethereum and Ripple, early warning signals were obtained prior to the crashes of each cryptocurrency, while for Litecoin the methodology did not work and was obtained a false positive. The authors tested their methodology with 8 other different time series and only 2 had false positives. This indicates to us that it would be worthwhile to research further into the reliability of this methodology to detect early signs of critical transitions in financial markets.

Figure 6 shows the log-price time series and the C^1 norms of the Bitcoin and Ethereum persistence landscapes, prior to the cryptocurrency crash, while figure 7 shows the clusters obtained with the k -means. At the end of each period, you can see how the time series of the C^1 norms have a peak.

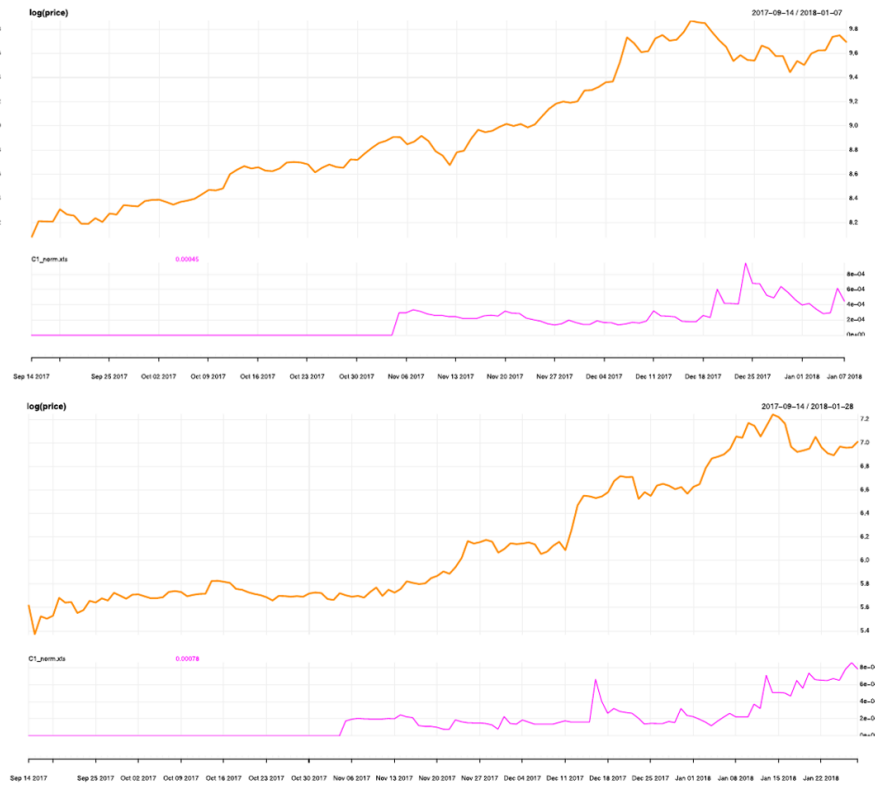


Figure 6: Bitcoin (up) and Ethereum (down) - Logarithm of the price and the C^1 norms of the persistence landscapes, respectively, prior to the cryptocurrency crash. Images taken from [10]

This article was published in May 2019 by Elsevier, and the author men-

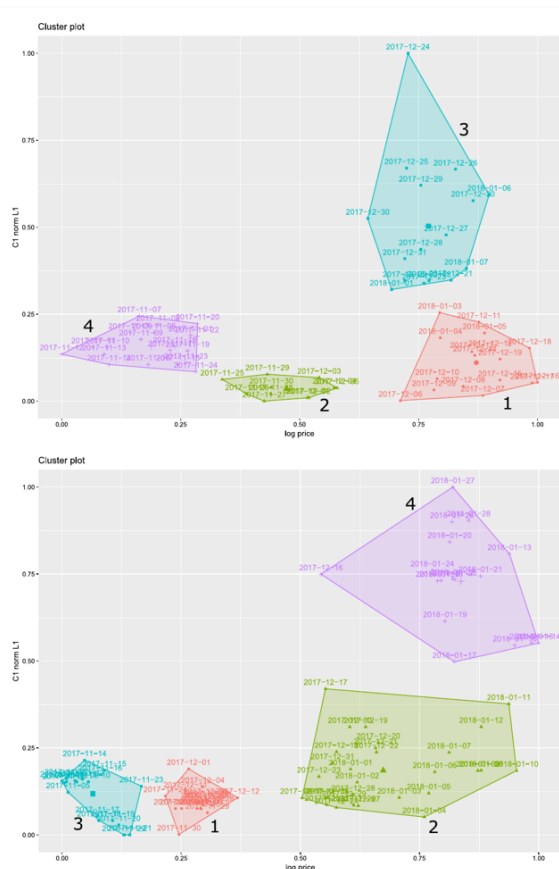


Figure 7: Bitcoin (up) and Ethereum (down) - Clusters obtained by applying the k -means algorithm. Cluster 3 gives a strong critical transition signal. Images taken from [10].

tioned that [9], [11] and [22] were the few research papers about TDA for financial data analysis. The major advantage of studying critical transitions in financial markets with TDA is that it is free of statistical assumptions in the time series.

4 Investing strategies based on a TDA indicator

In the financial asset management industry it is known that turbulent periods in financial markets are characterized by low returns, high volatility and the correlation between assets increases. This makes diversification —the golden rule in investing— not working as it should.

One way to deal with turbulent periods while investing is the estimation of the dynamic regime of financial markets —the behavior that the market has over time— or the creation of risk indicators that predict changes in the market regime. Both approaches allows us to create investment strategies with low risk and a higher return compared to the (*buy-and-hold strategy*) ([1]).

[1] designed three investment strategies via a persistent homology based turbulence index (PHTI) they created. In their research, they simulated these strategies using the PHTI index, the VIX index, and the [5] index based on the *Mahalanobis* distance —the two latter being known turbulence indices. The authors found that the PHTI-based strategies were better according to some performance measures described later.

The PHTI is constructed as follows. Let us fix N industrial portfolios and consider a sliding window of 60 trading days. This lead to a matrix of $60 \times N$ that contains in its columns the 60 daily returns of the N industrial portfolios. Then, we obtain the 1-dimensional (or 0-dimensional) persistence diagram via a Vietoris-Rips simplicial complex filtration.

Moving the sliding window, we obtain a set of persistence diagrams $\{P_t\}_t$, and then construct a sequence $\{W_t\}_t$, where W_t is the Wasserstein distance between P_t and P_{t-1} . $\{W_t\}_t$ is called the PHTI *raw* index. The sequence $\{W_t\}_t$ is smoothened with a moving average of 60 days and gives rise to the **PHTI** index $\{w_t\}_t$:

$$w_t = \frac{1}{60} \sum_{j=0}^{59} W_{t-j}.$$

[1] took into account in the investment strategies the last 60 monthly values of the PHTI. Depending on which quintile the last value falls into, it was the the total value of equity in the S&P500. The following were the three investment strategies the authors designed:

- 1) **Protection against extreme values of the index.** Investing of the 100 % during the following month unless the last value falls into the last quintile. In this last case, do not invest anything in that month.
- 2) **Flexible exposure.** If the last value falls in the n -th quintile, $n \in \{1, 2, \dots, 5\}$, then invest the $(100 - 20(n - 1))$ % of equity (100 %, 80 %, 60 %, 40 % and 20 % for $n = 1, 2, 3, 4, 5$, respectively).
- 3) **Exposure with leverage.** Leverage allows us to use debt to increase the amount of money for an investment. If the last value falls into the n -th quintile, $n \in \{1, 2, \dots, 5\}$, then invest the $(120 - 5n(n - 1))$ % of equity (120 %, 110 %, 90 %, 60 % and 20 % for $n = 1, 2, 3, 4, 5$, respectively).

[1] called this methodology the 60-60-60 rule because of the size of the sliding window, the size of the moving average, and the 60 monthly values of w_t considered for the investment strategies. For the other two turbulence indices, the 60-60-60 rule was adapted.

The authors in their simulations used $N = 10$ and $N = 30$ industrial portfolios from different sectors to represent the general market situation. We denote the PHTI that uses the 10 and 30 portfolios as PHTI(10) and PHTI(30), respectively. Analogously with the index of [5], denoted here by Chow(10) and Chow(30). This leads to 5 different turbulence indices: PHTI(10), PHTI(30), Chow(10), Chow(30) and VIX. Each of these indices can be used for the 3 different investment strategies described. These strategies were tested from June 1991 to June 2019, encompassing 337 monthly returns of the S&P500, and were compared to the buy-and-hold strategy as *benchmark*.

The authors used, as performance measures for any investment strategy, the mean annualized return μ , the mean annualized standard deviation of returns σ , the annualized Sharpe ratio SR (*Sharpe ratio*, quotient between the two previous measures), and the maximum *drawdown maxDD* (maximum drop experienced in the portfolio since the last maximum until this maximum is exceeded again).

In table 1 the 4 performance measures are reported. We can see that the PHTI(10) and the PHTI(30) are the indices that showed better Sharpe Ratios and lower maximum drawdowns in the 3 different strategies. In addition, they also perform better than the benchmark with respect to Sharpe Ratio and maximum drawdown. So the PHTI has the potential to be a good turbulence index.

5 A new version of Persistent Homology Based Index

Combining ideas of [10, 1], we propose another turbulence index based on persistent homology and tested it on daily log-returns of the SP500 between January 2, 2019, and April 07, 2020, in order to see if it is capable to detect early warning signals of the 2020 stock market crash on February 20, 2020, due to the COVID-19 pandemic, when a price drop of 33% started until March 23. The construction is the following. Let $\{x_t\}_t$ a time series of the log-returns of some financial asset. Through the Takens's embedding, we obtain a set of d -dimensional points

$$z_t := (x_t, x_{t+\tau}, \dots, x_{t+\tau(d-1)}) \in \mathbb{R}^d,$$

where τ is called the *time delay* of the embedding. In [10], the authors considered $\tau = 1$ and $d = 4$. In our experiment, we set $d = 3$ and $\tau = 2$, so each point could represent prices behaviour in a window of 5 trading days (a trading week).

With a window of $w = 60$ trading days, for each t we get a point cloud in \mathbb{R}^d

$$Z^t := \{z_t, z_{t+1}, \dots, z_{t+(w-1)}\},$$

Protection against extreme index values						
	Benchmark	PHTI(10)	PHTI(30)	Chow(10)	Chow(30)	VIX
μ	8.55	8.94	8.87	7.27	6.35	5.49
σ	14.18	10.74	10.84	11.92	11.77	10.04
SR	0.60	0.83	0.82	0.61	0.54	0.55
$maxDD$	52.56	33.42	33.42	41.09	44.43	39.47

Flexible exposure						
	Benchmark	PHTI(10)	PHTI(30)	Chow(10)	Chow(30)	VIX
μ	8.55	5.99	5.96	4.58	4.60	5.10
σ	14.18	8.32	8.53	9.02	8.81	7.98
SR	0.60	0.72	0.70	0.51	0.52	0.64
$maxDD$	52.56	24.75	26.43	35.98	35.97	35.00

Exposure with leverage						
	Benchmark	PHTI(10)	PHTI(30)	Chow(10)	Chow(30)	VIX
μ	8.55	8.12	8.28	6.46	6.31	6.26
σ	14.18	10.82	11.26	11.82	11.68	10.18
SR	0.60	0.75	0.74	0.55	0.54	0.62
$maxDD$	52.56	33.15	33.28	44.08	45.06	43.52

Table 1: Performance measures of the different investment strategies with the different indices. PHTI(10) and the PHTI(30) are the persistent homology based indices that showed better Sharpe Ratios and lower maximum drawdowns.

and obtain the 0-dimensional persistence diagrams, together with their persistence landscapes. Let $\{\lambda_t\}_t$ be the time series of persistence landscapes obtained by the 0-dimensional or 1-dimensional persistence diagrams. Following [1], in order to see how these persistence landscapes change with respect time t , we track the distances between the persistence landscape λ_t at time t and the persistence landscape λ_{t-T} T days before using the L_2 norm:

$$M_t := \|\lambda_{t-T} - \lambda_t\|_2,$$

for each $t \geq T$. In [1] the authors used $T = 1$, but here we used with $T = 5$ in order to compare persistence landscapes between a trading week of difference.

In figure 8, we find two plots with our new turbulence index $\{M_t\}_t$ using 0-dimensional persistence diagrams, and the closes prices of the SP500, respectively, between April 11, 2019 and April 06, 2020. The red dotted line corresponds to the beginning of the 2020 crash in February 20, 2020. The first orange dotted line is the last maximum of our turbulence index before February 20, and the second orange dotted line was the first day, February 24, 2020, where the last maximum was exceeded. The second orange line can be considered as the warning signal of the stock market crash because of its growing exceeding last maximum of the index in February 24, just two trading days after the beginning of the crash.

Notice in figure 8 how the distances M_t start to grow a lot when the SP500 had huge losses (35% between February 20 and March 23) because of the stock market crash in 2020.

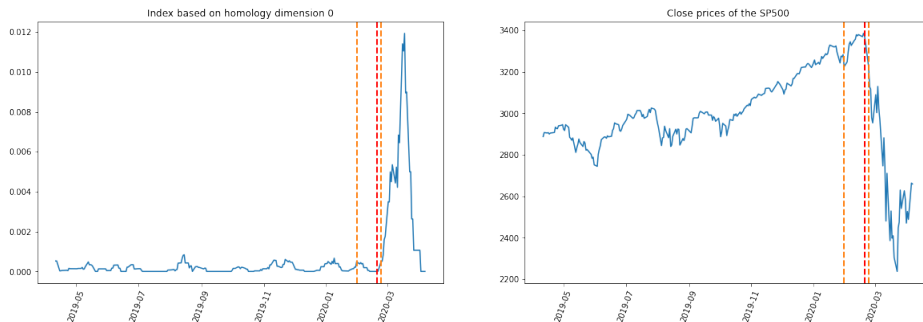


Figure 8: In the first plot, we find the new turbulence index $\{M_t\}_t$ using 0-dimensional persistence diagrams. The red dotted line corresponds to the beginning of the 2020 crash in February 20, 2020. The first orange dotted line is the last maximum of the index before February 20, and the second orange dotted line was the first day, February 24, 2020, where the last maximum was exceeded. In the second plot we find the close prices of the SP500 with the same dotted lines as the first plot. The time axis represent trading days between April 11, 2019 and April 06, 2020.

5.1 Comparing with Baitinger and Flegel (2019) index

Now, we compute Baitinger and Flegel (2019) index (see section 4) in order to see how well it warning us about the COVID induced financial crash in February 20, 2020, and compare it with our new index.

We consider $N = 10$ industrial portfolios¹ with daily returns between January 2, 2019 and April 07, 2020, and compute the 0-dimensional homology based PHTI(10) as in section 5. In figure 9 we can visualize the PHTI(10) and the close prices of the SP500 between June 24, 2019 and April 7, 2019. The red dotted line corresponds to the beginning of the 2020 crash in February 20, 2020. The first orange dotted line is the last maximum of the PHTI(10) before February 20, and the second orange dotted line was the first day, February 26, 2020, where the last maximum was exceeded. This latter line can be considered as a warning signal of the stock market crash, 4 trading days after the beginning of the crash, and two trading days after the warning signal given by our new turbulence index.

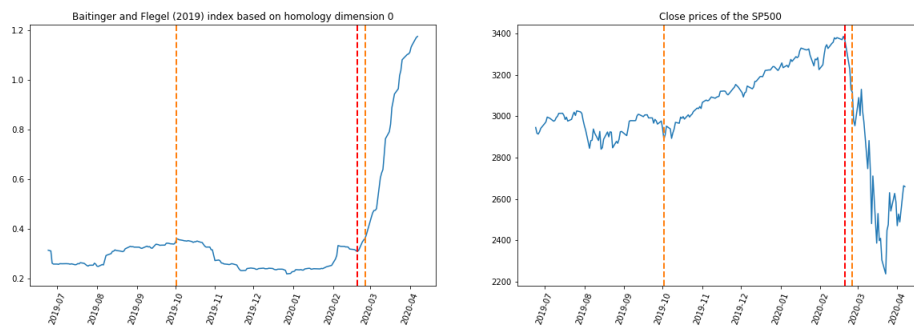


Figure 9: In the first plot, we find the PHTI(10) $\{w_t\}_t$ using 0-dimensional persistence diagrams. The red dotted line corresponds to the beginning of the 2020 crash in February 20, 2020. The first orange dotted line is the last maximum of the index before February 20, and the second orange dotted line was the first day, February 26, 2020, where the last maximum was exceeded. In the second plot we find the close prices of the SP500 with the same dotted lines as the first plot. The time axis represent trading days between April 11, 2019 and April 06, 2020.

All code and data we used can be found in a Github repository [18].

6 Conclusions

We reviewed some efforts that have been done to understand financial markets via TDA, specifically, [9, 11, 10, 1], and proposed a new turbulence index based

¹The source of the dataset was the Kenneth R. French Data Library. Click [here](#) for further information about the dataset.

on persistence landscapes of 0-dimensional persistence diagrams. The calculations of the persistent homology were done using the TDA Python library Giotto-TDA ([20]). Applications of TDA on financial markets are in their early stages of development at the time this research was done as [10] mentioned. Those applications have been focused on the detection of early warning signals of critical transition on financial markets (crashes of markets). The results are promising and indicates us that there is a room of collaboration between academic research and financial industry to explore TDA insights of financial markets.

Acknowledgements

This research was undertaken as part of a research fellowship given by CONACYT through the ‘*Sistema Nacional de Investigadores*’. I am thankful with Dr. José-Carlos Gómez-Larrañaga (CIMAT) for give me the opportunity of working with him and let me accomplish this research to know more about the behaviour of financial markets through new tools and points of view; and thankful with Jesús Rodríguez Viorato for his patience in reviewing this paper and contributing with his ideas and observations.

References

- [1] Eduard Baitinger and Samuel Flegel. The better turbulence index? forecasting adverse financial markets regimes with persistent homology. *Forecasting Adverse Financial Markets Regimes with Persistent Homology (November 20, 2019)*, 2019.
- [2] Jesse Berwald, Marian Gidea, and Mikael Vejdemo-Johansson. Automatic recognition and tagging of topologically different regimes in dynamical systems. *arXiv preprint arXiv:1312.2482*, 2013.
- [3] Peter Bubenik. Statistical topological data analysis using persistence landscapes. *The Journal of Machine Learning Research*, 16(1):77–102, 2015.
- [4] Gunnar Carlsson. Topology and data. *Bulletin of the American Mathematical Society*, 46(2):255–308, 2009.
- [5] George Chow, Eric Jacquier, Mark Kritzman, and Kenneth Lowry. Optimal portfolios in good times and bad. *Financial Analysts Journal*, 55(3):65–73, 1999.
- [6] David Cohen-Steiner, Herbert Edelsbrunner, and John Harer. Stability of persistence diagrams. *Discrete & computational geometry*, 37(1):103–120, 2007.
- [7] Herbert Edelsbrunner and John Harer. Persistent homology - A survey. *Contemporary mathematics*, 453:257–282, 2008.

- [8] Herbert Edelsbrunner and John Harer. *Computational topology - an introduction*. American Mathematical Soc., 2010.
- [9] Marian Gidea. Topological data analysis of critical transitions in financial networks. In *International Conference and School on Network Science*, pages 47–59. Springer, 2017.
- [10] Marian Gidea, Daniel Goldsmith, Yuri Katz, Pablo Roldan, and Yonah Shmalo. Topological recognition of critical transitions in time series of cryptocurrencies. *Physica A: Statistical Mechanics and its Applications*, page 123843, 2020.
- [11] Marian Gidea and Yuri Katz. Topological data analysis of financial time series: Landscapes of crashes. *Physica A: Statistical Mechanics and its Applications*, 491:820–834, 2018.
- [12] Danijela Horak, Slobodan Maletić, and Milan Rajković. Persistent homology of complex networks. *Journal of Statistical Mechanics: Theory and Experiment*, 2009(03):P03034, 2009.
- [13] Anil K Jain. Data clustering: 50 years beyond k-means. *Pattern recognition letters*, 31(8):651–666, 2010.
- [14] Alexander J McNeil, Rüdiger Frey, and Paul Embrechts. *Quantitative risk management: concepts, techniques and tools-revised edition*. Princeton university press, 2015.
- [15] Nina Otter, Mason A Porter, Ulrike Tillmann, Peter Grindrod, and Heather A Harrington. A roadmap for the computation of persistent homology. *EPJ Data Science*, 6:1–38, 2017.
- [16] Jose A Perea and John Harer. Sliding windows and persistence: An application of topological methods to signal analysis. *Foundations of Computational Mathematics*, 15(3):799–838, 2015.
- [17] Nalini Ravishanker and Renjie Chen. Topological data analysis (TDA) for time series. *arXiv preprint arXiv:1909.10604*, 2019.
- [18] Miguel Ruiz. Tda financial markets. https://github.com/miguelruor/TDA_financial_markets, 2022.
- [19] Floris Takens. Detecting strange attractors in turbulence. In *Dynamical systems and turbulence, Warwick 1980*, pages 366–381. Springer, 1981.
- [20] Guillaume Tauzin, Umberto Lupo, Lewis Tunstall, Julian Burella Pérez, Matteo Caorsi, Anibal Medina-Mardones, Alberto Dassatti, and Kathryn Hess. giotto-tda: A topological data analysis toolkit for machine learning and data exploration, 2020.

- [21] Robert R Trippi and Jae K Preface By-Lee. *Artificial intelligence in finance and investing: state-of-the-art technologies for securities selection and portfolio management*. McGraw-Hill, Inc., 1995.
- [22] Patrick Truong. An exploration of topological properties of high-frequency one-dimensional financial time series data using tda, 2017.